26th EPS Conf. on Contr. Fusion and Plasma Physics, Maastricht, 14 - 18 June 1999 ECA Vol.23J (1999) 1669 - 1672

Turbulence Suppression by $\mathbf{E} \times \mathrm{B}$ Shear in JET Optimized Shear Pulses

M. A. Beer[1], R. V. Budny[1], C. D. Challis, G. Conway, C. Gormezano, G. Rewoldt[1], A. C. C. Sips, F. X. Söldner, B. J. D. Tubbing, and M. Von Hellerman

JET Joint Undertaking, Abingdon, OX14 3EA, UK
[1]*Princeton University Plasma Physics Laboratory, Princeton, NJ 08543, USA*

We calculate microinstability growth rates in JET optimized shear plasmas with a comprehensive gyrofluid model, including sheared $\mathbf{E} \times \mathbf{B}$ flows, trapped electrons, and all dominant ion species in realistic magnetic geometry. We find good correlation between $\mathbf{E} \times \mathbf{B}$ shear suppression of microinstabilities and both the formation and collapse of the internal transport barrier.

I. Introduction

Suppression of turbulence by $\mathbf{E} \times \mathbf{B}$ shear is a leading candidate for understanding the mechanism of transport improvement in L-H transitions and in the formation of internal transport barriers. However, most of the evidence supporting this view is somewhat qualitative. Usually, one expects turbulence suppression when ω_E, the $\mathbf{E} \times \mathbf{B}$ shearing rate, is on the order of the linear growth rate or a turbulent decorrelation time. Many investigations of this nature use simplified estimates of the linear growth rate or approximate models to include the flow shear. In this work we extend these studies by calculating the microinstability growth rates with a comprehensive numerical gyrofluid calculation evolving the dynamics of the main ion species, impurities, beams, and trapped electrons. We also now include the sheared $\mathbf{E} \times \mathbf{B}$ flow directly in the calculation of the instability growth rates.

II. Incorporating sheared $\mathbf{E} \times \mathbf{B}$ flows in gyrofluid simulations

We have included the effects of equilibrium sheared $\mathbf{E} \times \mathbf{B}$ flows in our gyrofluid simulations the following manner. In each fluid equation, $\mathbf{E} \times \mathbf{B}$ convection gives rise to three terms:

$$\frac{\partial n}{\partial t} + \mathbf{v}_E^{(0)} \cdot \nabla n + \mathbf{v}_E \cdot \nabla n_0 + \mathbf{v}_E \cdot \nabla n + \cdots = 0, \tag{1}$$

corresponding to a sheared equilibrium $\mathbf{E}^{(0)} \times \mathbf{B}$ flow, a linear convection of the equilibrium density gradient by the perturbed $\mathbf{E}$, and an $\mathbf{E} \times \mathbf{B}$ nonlinearity. In our flux-tube simulations, we solve the evolution of the fluid quantities in general geometry, in a flux-tube aligned with the magnetic field, $n(\alpha, \psi, \theta, t)$, where α and ψ are coordinates perpendicular to the field, $\mathbf{B} = \nabla\alpha \times \nabla\psi$, ψ is the poloidal flux, and θ measures distance along the field line. In these coordinates Eq. (1) becomes:

$$\frac{\partial n}{\partial t} - c\frac{\partial \phi^{(0)}}{\partial \psi}\frac{\partial n}{\partial \alpha} + c\frac{\partial \phi}{\partial \alpha}\frac{\partial n_0}{\partial \psi} + c\left(\frac{\partial \phi}{\partial \alpha}\frac{\partial n}{\partial \psi} - \frac{\partial \phi}{\partial \psi}\frac{\partial n}{\partial \alpha}\right) + \cdots = 0. \tag{2}$$

For a linearly sheared $\mathbf{E}^{(0)} \times \mathbf{B}$ flow, $\partial\phi^{(0)}/\partial\psi = \partial^2\phi^{(0)}/\partial\psi^2(\psi - \psi_0)$, where ψ_0 is the poloidal flux at the center of the flux-tube simulation domain. The constant $\mathbf{E}^{(0)} \times \mathbf{B}$ flow only introduces a doppler shift, and is not included here. By introducing the variable transformation $\alpha' = \alpha - c\partial^2\phi^{(0)}/\partial\psi^2(\psi - \psi_0)t$, so the new coordinates shear in the poloidal direction with the

equilibrium flow, the $\mathbf{v}_E^{(0)} \cdot \nabla n$ term is introduced, consistent with smooth statistically periodic boundary conditions across the ψ domain. In other words, an eddy which is convected out one side of the flux-tube will re-enter the other side with the appropriate rotation so it does not feel a discontinuity. The only change is that now radial derivatives are time dependent:

$$\frac{\partial}{\partial \psi} = \frac{\partial}{\partial \psi'} - c\frac{\partial^2 \phi^{(0)}}{\partial \psi^2} t \frac{\partial}{\partial \alpha}. \tag{3}$$

In more standard ballooning notation, this means that the θ_0's shift: $\theta_0' = \theta_0 + \Omega_E t/\hat{s}$, where $k_r = k_\theta \hat{s} \theta_0$, and $\Omega_E = (e/T_i)\partial^2\phi^{(0)}/\partial\rho^2$, and ρ is a normalized flux surface label.

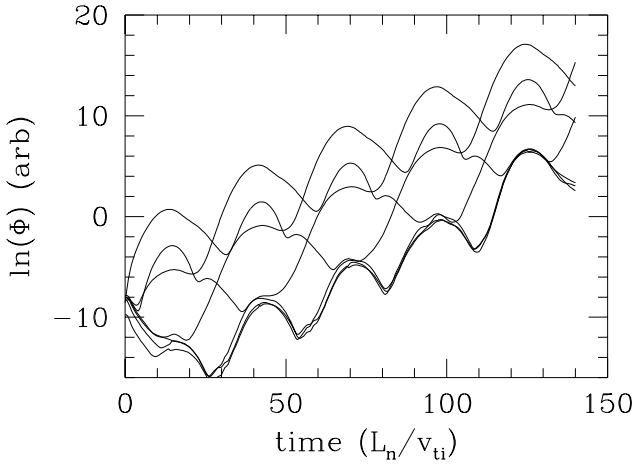

Fig. 1. $\Phi(t)$ for seven $\theta_0's$ in the presence of $\mathbf{E} \times \mathbf{B}$ shear. In this representation the addition of flow shear introduces oscillations on top of exponential growth, and a reduced effective growth rate.

The linear behavior of our initial value calculations with flow shear is shown in Fig. 1. When a mode is sheared to sufficiently high θ_0, we reintroduce it at negative θ_0, to resolve the physically relevant part of k-space. Different θ_0's are linearly coupled through the boundary condition along the field line,[1] making the linear calculation with flow shear 2D. This makes the linear computations more challenging, increasing the importance of the relative speed of our fluid model. The net growth now depends in some sense on the θ_0 averaged growth rate, as a mode is convected poloidally. This approach and our results are similar to Ref. 2. The potentially destabilizing effect of parallel flow shear is not included.

In the analysis that follows, we use bounce averaged trapped electron fluid equations[3] coupled with the toroidal ion gyrofluid equations[4] for D, an impurity, and beams, in the electrostatic approximation. This model thus includes both the long wavelength TEM and ITG instabilities, and has been thoroughly benchmarked against fully kinetic calculations.[5]

Because the details of the magnetic geometry can significantly affect the results, we solve these equations in realistic geometry. The details of flux-tube simulation in general geometry are given in Ref. 1. Using measured profiles from TRANSP,[6] we numerically calculate the equilibrium at each time of interest, and then calculate the necessary geometrical coefficients, e.g. the ∇B and curvature drifts, using techniques in Ref. 7.

III. Detailed comparison with JET optimised shear pulse

We now analyze JET optimized shear discharge 40847,[8] which is a stringent testbed for the $\mathbf{E} \times \mathbf{B}$ shear suppression paradigm. Shortly after the beams turn on at $t = 5$s, an internal

transport barrier forms and T_i increases sharply, as shown in Fig. 2(a), and χ_i, calculated by TRANSP, drops, shown in Fig. 2(b). At $t = 6.8$s, the edge undergoes an L-H transition, and core confinement deteriorates. However, within the time resolution of the data, we cannot determine whether the L-H transition precedes the loss of the core ITB, or whether the loss of the core ITB precedes the L-H transition. Likewise, we cannot determine whether the loss of core rotation precedes the loss of the core ITB, or vice versa. It is also a possibile that the core ITB collapse is triggered by MHD.

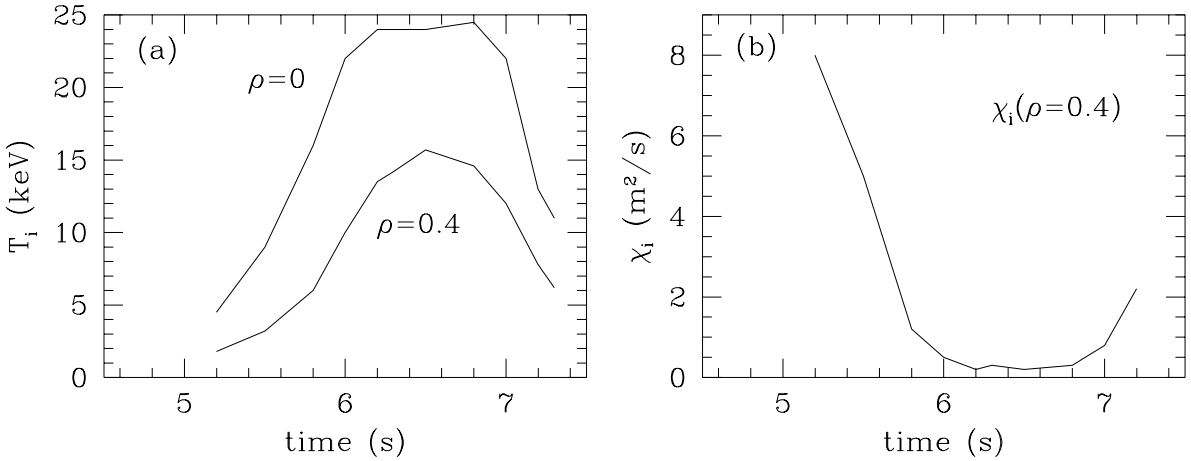

Fig. 2. (a) T_i and (b) $\chi_i(\rho = 0.4)$ for a JET optimized shear discharge. At $t = 6.8$s the core ITB collapses.

To analyze this discharge we use profiles from TRANSP and their gradients as inputs at the flux surface of interest. E_r is calculated from radial force balance using the NCLASS package,[9] using measured v_ϕ and ∇p profiles and calculating the neoclassical v_θ. For this discharge the contribution from v_ϕ dominates E_r. The time behavior of the measured v_ϕ and calculated shearing rate, ω_E, are shown in Fig. 3. After $t = 6.8$s, rotation slows and ω_E drops.

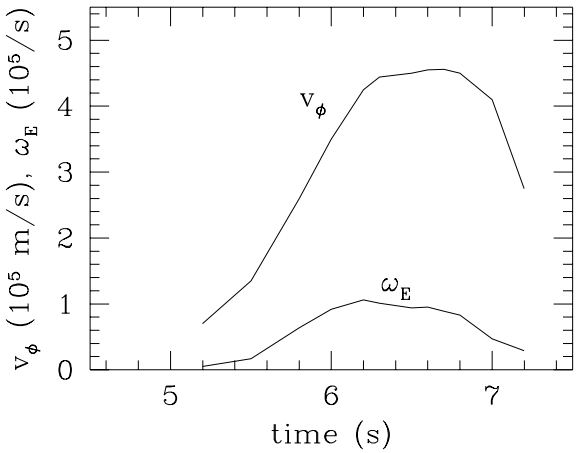

Fig. 3. Toroidal rotation at $R = 340$cm, v_ϕ, and the shearing rate at $\rho = 0.4$, ω_E, vs. time. After $t = 6.8$s, core rotation slows and ω_E drops.

Fig. 4 shows the growth rate vs. time at $\rho = 0.4$, maximized over $k_\theta \rho_i < 1.5$. We first show the growth rate ignoring $\mathbf{E} \times \mathbf{B}$ shear, labelled $\gamma_{E=0}$. As the profiles steepen, the growth rates first increase and then decrease, although this does not appear to be due to geometrical finite-β

stabilization,[10] in contrast to ERS on TFTR. This was tested by recalculating the equilibria with β reduced by a factor of 10, and repeating the growth rate calculation with the new geometry but the same driving gradients, and little change was found. As the growth rates drop, toroidal rotation builds up until the shearing rate, ω_E, is within a factor of 2 of the linear growth rate. This occurs near $t = 6.2$s, roughly consistent with the decrease in χ_i shown in Fig. 2. Later, toroidal rotation decreases and ω_E drops below $\gamma_{E=0}$ at around $t = 7$s. This is also consistent with the increase in χ_i in Fig. 2, and the loss of the internal transport barrier.

Finally in Fig. 4 we show the growth rates including $\mathbf{E} \times \mathbf{B}$ shear, labelled γ_{full}. These are very roughly consistent with the expectation of complete linear stability when $\omega_E > \gamma_{E=0}$, and even more consistent with both the formation of the internal transport barrier, and the loss of the core barrier at $t = 6.8$s. These results encourage fully nonlinear simulations of this discharge in the future, using the technique presented above.

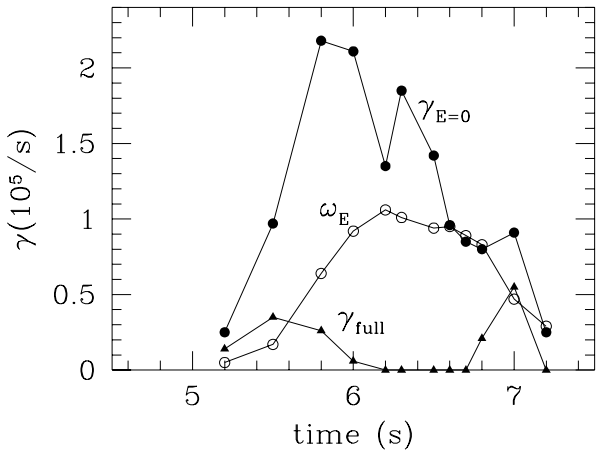

Fig. 4. Growth rates and shearing rates vs. time at the $\rho = 0.4$ surface, calculated with and without $\mathbf{E} \times \mathbf{B}$ shear. At $t = 6$s the shearing rate has increased to within a factor of 2 of the linear growth rate ignoring $\mathbf{E} \times \mathbf{B}$ shear, $\gamma_{E=0}$. Later, toroidal rotation slows and ω_E drops below $\gamma_{E=0}$. The full linear growth rates including $\mathbf{E} \times \mathbf{B}$ shear, labelled γ_{full}, correlate well with the reduction in χ_i as the barrier is formed, and the increase in χ_i as the barrier collapes.

Acknowledgments

We thank the JET team for providing the data and useful discussions, W. Dorland and G. Hammett for discussions and significant code development, and J. Manickam for providing the equilibrium solver. This work was supported by U.S.DOE Contract No. DE AC02-76CO3073.

[1]M. A. Beer, S. C. Cowley, and G. W. Hammett, Phys. Plasmas **2**, 2687 (1995).
[2]R. E. Waltz, R. L. Dewar, and X. Garbet, Phys. Plasmas **5**, 1784 (1998).
[3]M. A. Beer and G. W. Hammett, Phys. Plasmas **3**, 4018 (1996).
[4]M. A. Beer and G. W. Hammett, Phys. Plasmas **3**, 4046 (1996).
[5]G. Rewoldt, *et al.*, Phys. Fluids **25**, 480 (1982) and **30**, 807 (1987).
[6]R. V. Budny, H. Biglari, M. G. Bell, *et al.*, Nucl. Fusion **32**, 429 (1992).
[7]C. M. Bishop, P. Kirby, J. W. Connor, R. J. Hastie, J. B. Taylor, Nucl. Fusion **24** 1579 (1984).
[8]C. Gormezano, Y. F. Baranov, C. D. Challis, *et al.*, Phys. Rev. Lett. **80**, 5544 (1998).
[9]W. A. Houlberg, K. C. Shaing, *et al.*, Phys. Plasmas **4**, 3230 (1998).
[10]M. A. Beer, G. W. Hammett, G. Rewoldt, *et al.*, Phys. Plasmas **4**, 1792 (1997).